Acta Oceanol. Sin., 2018, Vol. 37, No. 11, P. 68–76
DOI: 10.1007/s13131-018-1334-x
http://www.hyxb.org.cn
E-mail: hyxbe@263.net

The influence of up-wave barge motion on the water resonance at a narrow gap between two rectangular barges underwaves in the sea

JIN Ruijia[1, 2], NING Dezhi[1]*, BAI Wei[3], GENG Baolei[2]

[1] State Key Laboratory of Coastal and Offshore Engineering, Dalian University of Technology, Dalian 116024, China

[2] National Engineering Laboratory for Port Hydraulic Construction Technology, Tianjin Research Institute for Water Transportation Engineering, Tianjin 300456, China

[3] School of Computing, Mathematics and Digital Technology, Manchester Metropolitan University, Manchester M1 5GD, UK

Received 4 August 2017; accepted 10 October 2017

Abstract

A three-dimensional time-domain potential flow model is developed and applied to simulate the wave resonance in a gap between two side-by-side rectangular barges. A fourth-order predict-correct method is implemented to update free surface boundary conditions. The response of an up-wave barge is predicted by solving the motion equation with the Newmark-β method. Following the validation of the developed numerical model for wave radiation and diffraction around two side-by-side barges, the influence of up-wave barge motion on the gap surfaceresonance is investigated in two different locations of the up-wave barge relative to the back-wave barge at various frequencies. The results reveal that the freely floating up-wave barge significantly influences the resonance frequency and the resonance wave amplitude. Simultaneously, the up-wave barge located in the middle of the back-wave barge leads to a reduction in the resonance wave amplitude and motion response when compared with other configurations.

Key words: side-by-side barges, gap resonance, time-domain model, up-wave barge motion

Citation: Jin Ruijia, Ning Dezhi, Bai Wei, Geng Baolei. 2018. The influence of up-wave barge motion on the water resonance at a narrow gap between two rectangular barges underwaves in the sea. Acta Oceanologica Sinica, 37(11): 68–76, doi: 10.1007/s13131-018-1334-x

1 Introduction

Recently, the fast development of ocean engineering has led to the increasing attention on hydrodynamic research on the narrow gap between two floating structures due to the possible violent resonance phenomenon of the fluid within the narrow gap. In reality, the two-body system can correspond to ship-to-ship cargo transfer, a liquefied natural gas (LNG) carrier alongside a terminal and offloading from a floating production storage and offloading (FPSO).

With respect to the fluid resonance between two side-by-side barges, several pioneering studies focused on two-dimensional configurations by assuming the gap of infinite length. In the framework of the potential flow theory, the wave interaction with two adjacent rectangular barges were modelled by Newman and Sclavounos (1988) and the high wave elevations in the narrow gap between the barges as well as the large hydrodynamic forces were reported. Miao et al. (2000, 2001) studied the influence of the gap between two fixed rectangular caissons on wave forces using the boundary element method. The results indicate that the resonance wave forces on each caisson could be several times the forces on an isolated caisson. In addition, a theoretical analysis was also performed by Miao et al. (2000, 2001) to demonstrate the occurrence of resonance.

However, it is well known that the gap resonance is simulated as over-predicted by the potential flow theory owing to the ignorance of fluid viscosity. Lu and Chen (2012) estimated the associated dissipation coefficient obtained by the equivalence ofdissipated force and friction force. For the purpose of suppressing the inaccurate resonanceamplitude in the narrow gap, a straightforward investigation of the gap resonance problem might use the viscous fluid model by solving the Navier-Stokes equation. Lu et al. (2010) examined the fluid resonance between three identical bodies with two narrow gaps by a numerical method based on the aforementioned method, and the results were in good agreement with the experimental data reported by Iwata et al. (2007). In the numerical model proposed by Kristiansen and Faltinsen (2012), the computational domain for the Navier-Stokes solver was fully submerged in the fluid to capture the viscous effects, while the free surface was simulatedusing the potential flow theory. Moradi et al. (2015) applied OpenFOAM to study the influence of the gap inlet configuration on the resonance wave amplitude and frequency. Additionally, the geometrical properties of the fixed bodies significantly influence gap resonance characteristics. Jiang et al. (2017) examined the influence of the heaving frequency and amplitude with respected to various moonpool configurations on fluid resonance behavior by employing a two-

Foundation item: The Research Innovation Foundation of Tianjin Research Institute for Water Transportation Engineering of China under contract No. TKS 170215; the Research Foundation of State Key Laboratory of Coastal and Offshore Engineering of Dalian University of Technology of China under contract No. TKS 170215.

*Corresponding author, E-mail: dzning@dlut.edu.cn

dimensional numerical wave flume based on OpenFOAM package with Re-Normalization Group (RNG) turbulent model. To utilize the efficiency of the potential flow theory, an artificial damping was introduced in the potential flow theory, including linear damping terms by Newman (2004) and a linear dissipative term in the free surface boundary condition by Chen (2004). The method proposed by Chen was employed by other scholars including Pauw et al. (2007), Bunnik et al. (2009) and Lu et al. (2011), and good agreements between numerical predictions and experimental data were observed. In addition, several scholars investigated the issue by a semi-analytical solutionin order to study the fluid resonance in the gap simply and effectively, for instance, Miao et al. (2001), Yeung and Seah (2006) and Liu and Li (2014).

However, the aforementioned two-dimensional (2-D) models are limited in capturing the real three-dimensional (3-D) characteristics of the fluid in the gap. With respect to the 3-D situation, Molin et al. (2010) performed experiments to recordcenterline wave elevations in the narrow gap between two fixed rectangular barges in waves, and the results were widely used in numerical model validation. In the 3-D numerical simulation, the potential flow theory model is applied owing to the huge calculation of the viscous flow theory model, for example, Sun et al. (2010), Watai et al. (2015), Perić and Swan (2015) and Jin et al. (2017). Specifically, Perić and Swan (2015) also experimentally examined the wave excitation in the gap between two adjacent bodies and provided a detailed description of the spatial variation of the water surface elevation in the gap between a fixed body and a floating body. Feng and Bai (2015) applied a fully nonlinear potential flow model to investigate the wave resonances in the gap between two side-by-side barges in beam seas, in which the main focus was put on the nonlinear behaviors and the stiff/soft spring properties of the gap resonances. Furthermore, a second-order potential flow model was applied in Jin et al. (2017) to investigate the influence of wave directionality on the gap resonance, and the results revealed that the incident wave angleonly affected the resonance wave amplitude, but not the resonance frequency.

Most previous numerical studies on the gap resonance between 2-D or 3-D barges were limited to the fixed ones. However, in reality, the up-wave barge may be free to move in waves. For instance, when the LNG carrier and the FPSO are in close proximity, the FPSO is considered as fixed due to its huge volume and mass while the LNG carrier is expected to respond to the wave action. Studies focused on the gap resonance between two moving barges in the 2-D situation. Fredriken et al. (2014) investigated the behavior of piston-mode resonance in the moonpool at low forward/ incoming current speeds. Li and Teng (2015) studied the coupled effects of roll motion and fluid resonance between two rectangular barges based on a CFD package OpenFOAM. The results indicated that the resonance frequency of the fluid in the narrow gap between two rolling barges decreased when compared to that between two fixed barges, but the resonance wave height appeared to be in the same magnitude.

However, there is a paucity of numerical investigations on the gap resonance in the gap between 3-D side-by-side moving barges, and it is important to improve the understanding of the 3-D problem requirements. Therefore, the aim of the present study involves examining the influence of up-wave barge motion on the wave resonance in the gap between two 3-D side-by-side barges. In order to achieve this, a time domain potential flow model is developed and applied. In the numerical model, the waves in a circular computational domain with the structure at its center are simulated. A damping zone is placed on the free surface at the outskirts of the domain to absorb the outgoing scattering wave. The developed numerical model is first validated by wave radiation and diffraction problems. The wave elevation in the gap and motion response of the up-wave barge over various incident wave frequencies are discussed. Furthermore, the influences of the up-wave barge location on the hydrodynamic characteristics of the two-body system are also assessed in this study.

2 Mathematical formulation

For the purposes of studying the wave-structure interaction problem, a numerical simulation is performed in a circular fluid domain, as shown in Fig. 1. An annulus damping zone is used to dissipate the scattered wave energy to satisfy the radiation boundary condition. The origin of the coordinate system *Oxyz* is placed at the center of the gap on the still water surface with the z-axis pointing upwards and the x-direction parallel to the gap. The incident wave angle (denoted by β) is measured from the positive x-direction in the counterclock direction and the damping zone exhibits a width of one wavelength.

In the time domain model, the fluid is assumed as ideal, i.e., inviscid and irrotational in the fluid domain, and thus the flow velocity potential satisfies the Laplace equation and boundary conditions. In this study, the velocity potential is decomposed into the incident potential ϕ_i and scattered potential ϕ_s. Thus, the scattered potential satisfies the Laplace equation in the domain as follows:

$$\nabla^2\phi_s = 0. \tag{1}$$

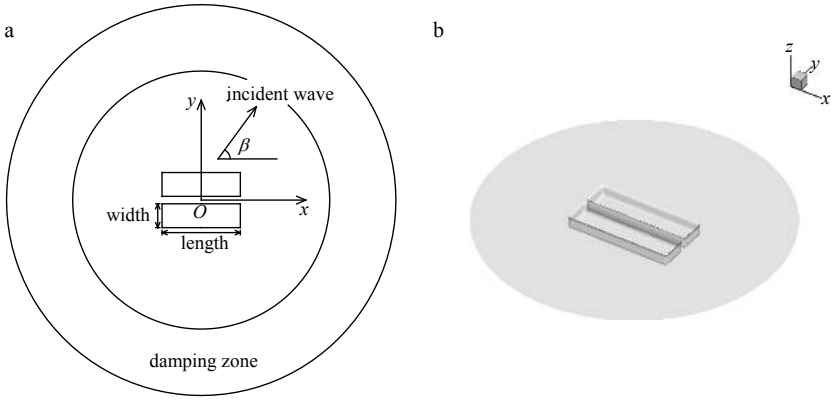

Fig. 1. Computational domain for wave interaction with two side-by-side rectangular barges. a. Plan view, and b. 3-D view.

It is subjected to the body boundary condition:

$$\frac{\partial \phi_{\mathrm{s}}}{\partial \vec{n}} = -\frac{\partial \phi_{\mathrm{i}}}{\partial \vec{n}} + f_{\mathrm{b}}, \tag{2}$$

where $\vec{n}$ denotes the unit normal vector, pointing out the fluid; f_{b} denotes the forcing term of the body boundary condition as follows:

$$f_{\mathrm{b}} = \left(\dot{\vec{\xi}} + \dot{\vec{\alpha}} \times (\vec{x} - \vec{x}_0)\right) \cdot \vec{n}, \tag{3}$$

with respect to the freely floating up-wave barge, $\vec{\xi} = (\xi_1,\ \xi_2,\ \xi_3)$; and $\vec{\alpha} = (\alpha_1,\ \alpha_2,\ \alpha_3) = (\xi_4,\ \xi_5,\ \xi_6)$ denote the translation and rotation motion of the moving barge, respectively, $\vec{x}_0$ denotes the rotation center;

$$f_{\mathrm{b}} = 0, \tag{4}$$

with respect to the fixed back-wave barge.

Linear kinematic and dynamic free surface boundary conditions are

$$\frac{\partial \eta_{\mathrm{s}}}{\partial t} = \frac{\partial \phi_{\mathrm{s}}}{\partial z}, \tag{5}$$

$$\frac{\partial \phi_{\mathrm{s}}}{\partial t} = -g\eta_{\mathrm{s}}, \tag{6}$$

where η_{s} denotes the scattered wave elevation, and g denotes the gravity acceleration.

To numerically solve the boundary value problem, we employ a Rankine source and its image about the seabed as the Green's function:

$$G(\vec{x}_{\mathrm{r}}, \vec{x}_{\mathrm{r0}}) = -\frac{1}{4\pi}\left(\frac{1}{R} + \frac{1}{R_1}\right), \tag{7}$$

where $\vec{x}_{\mathrm{r0}} = (x_{\mathrm{r0}}, y_{\mathrm{r0}}, z_{\mathrm{r0}})$ and $\vec{x}_{\mathrm{r}} = (x_{\mathrm{r}}, y_{\mathrm{r}}, z_{\mathrm{r}})$ denote the source point and the field point, respectively, and

$$\left.\begin{aligned} R &= \sqrt{(x_{\mathrm{r}} - x_{\mathrm{r0}})^2 + (y_{\mathrm{r}} - y_{\mathrm{r0}})^2 + (z_{\mathrm{r}} - z_{\mathrm{r0}})^2} \\ R_1 &= \sqrt{(x_{\mathrm{r}} - x_{\mathrm{r0}})^2 + (y_{\mathrm{r}} - y_{\mathrm{r0}})^2 + (z_{\mathrm{r}} + z_{\mathrm{r0}} + 2d)^2} \end{aligned}\right\}. \tag{8}$$

The second theorem of Green is applied to the scattered potential and Green's function, and thus the above boundary value problem is converted to the following boundary integral equation:

$$\alpha_{\mathrm{r}}\phi_{\mathrm{s}}(\vec{x}_{\mathrm{r0}}) = \iint_S \left[\phi_{\mathrm{s}}(\vec{x}_{\mathrm{r}})\frac{G(\vec{x}_{\mathrm{r}}, \vec{x}_{\mathrm{r0}})}{\partial \vec{n}} - G(\vec{x}_{\mathrm{r}}, \vec{x}_{\mathrm{r0}})\frac{\partial \phi_{\mathrm{s}}(\vec{x}_{\mathrm{r}})}{\partial \vec{n}}\right] \mathrm{d}S, \tag{9}$$

where α_{r} denotes the solid angle coefficient, which is dependent on the surface shape of the body surface. A higher-order boundary element method is used to numerically solve the boundary integral equation on eight-node quadrilateral elements.

In the calculation, the normal derivative of thescattered potential on the body surface and scattered potential on the free surface are known, and thus the scattered potential on the body surface and the normal derivative of the scattered potential on the free surface are obtained by solving integral Eq. (9).

Once the velocity potential on the body surface is obtained, the wave forces on a body can be computed by integrating the fluid pressure over the mean body surface. The total force can be divided into two terms:

$$\vec{F} = \vec{F}_{\mathrm{E}} + \vec{F}_{\mathrm{R}}, \tag{10}$$

where the exciting force is expressed as

$$\vec{F}_{\mathrm{E}} = -\rho \iint_{S_{\mathrm{b}}} \phi_{\mathrm{t}} \vec{n} \mathrm{d}s, \tag{11}$$

and the form of restoring force is

$$\begin{aligned} F_{\mathrm{R}} &= -\rho g \iint_{S_{\mathrm{b}}} \{[\xi_3 + \xi_4(y - y_0) - \xi_5(x - x_0)]\vec{n} + z\vec{\alpha} \times \bar{n}\} \mathrm{d}s \\ &= -\rho g A_{\mathrm{wp}}[\xi_3 + \xi_4(y_{\mathrm{f}} - y_0) - \xi_5(x_{\mathrm{f}} - x_0)]\vec{k}. \end{aligned} \tag{12}$$

where ρ denotes the fluid density, A_{wp} denotes the area of mean water-plane surface, $(x_{\mathrm{f}}, y_{\mathrm{f}})$ denotes the coordinates of the center of mean water-plane surface when the body is at rest and $\vec{k}$ denotes the unit vector in the z direction. It is noted that the restoring force is 0 for fixed bodies.

Furthermore, the motion equation is required fora floating body as follows:

$$\boldsymbol{M}\left\{\ddot{\vec{\xi}}\right\} + \boldsymbol{B}\left\{\dot{\vec{\xi}}\right\} + \boldsymbol{C}\left\{\vec{\xi}\right\} = \left\{\vec{F}_{\mathrm{E}}\right\}, \tag{13}$$

where $\boldsymbol{M}$ denotes the generalized body mass matrix, $\boldsymbol{B}$ denotes the viscous damping matrix and $\boldsymbol{C}$ denotes the restoring force matrix.

In the time domain, the simulation is advanced by using a time marching scheme. The detailed procedure used here includes the following steps.

Step 1: At time t, in the case of themoving body, the displacement $\vec{\xi}(t)$, velocity $\dot{\vec{\xi}}(t)$ and acceleration $\ddot{\vec{\xi}}(t)$ are known. On the free surface, the wave elevation $\eta_{\mathrm{s}}(t)$ and velocity potential $\phi_{\mathrm{s}}(t)$ are also known from the previous time step, the kinematic and dynamic free surface boundary conditions can thus be written in a general form as follows:

$$\left.\begin{aligned} \frac{\partial \phi_{\mathrm{s}}}{\partial t} &= f(\phi_{\mathrm{s}}, \eta_{\mathrm{s}}, t) \\ \frac{\partial \eta_{\mathrm{s}}}{\partial t} &= g(\phi_{\mathrm{s}}, \eta_{\mathrm{s}}, t) \end{aligned}\right\}. \tag{14}$$

Step 2: At time $t+\Delta t$, the displacement $\vec{\xi}(t+\Delta t)$, velocity $\dot{\vec{\xi}}(t+\Delta t)$ and acceleration $\ddot{\vec{\xi}}(t+\Delta t)$ for the moving body motion are predicted by the unconditional stable Newmark-β method as follows:

$$\left.\begin{aligned} \ddot{\vec{\xi}}(t+\Delta t) &= \ddot{\vec{\xi}}(t) \\ \xi(t+\Delta t) &= \xi(t) + \Delta t\dot{\vec{\xi}}(t) + 0.25 \times \Delta t^2\ddot{\vec{\xi}}(t) + \\ &\qquad 0.25 \times \Delta t^2\ddot{\vec{\xi}}(t+\Delta t) \\ \dot{\vec{\xi}}(t+\Delta t) &= \dot{\vec{\xi}}(t) + 0.5 \times \Delta t\ddot{\vec{\xi}}(t) + 0.5 \times \Delta t\ddot{\vec{\xi}}(t+\Delta t) \end{aligned}\right\}. \tag{15}$$

The fourth-order Adams-Bashforth method is used to predict the wave elevation and velocity potential on the free surface as follows:

$$\left.\begin{aligned}\phi_s(t+\Delta t) &= \phi_s(t)+\frac{\Delta t}{24}\left[55f(t)-59f(t-\Delta t)+\right.\\ &\left.37f(t-2\Delta t)-9f(t-3\Delta t)\right]\\ \eta_s(t+\Delta t) &= \eta_s(t)+\frac{\Delta t}{24}\left[55g(t)-59g(t-\Delta t)+\right.\\ &\left.37g(t-2\Delta t)-9g(t-3\Delta t)\right]\end{aligned}\right\}. \quad (16)$$

Step 3: At time t+Δt, the integral equation is implemented, and the velocity potential on the body surface and the normal derivative of potential on the free surface are obtained. The obtained normal derivative of the potential on the free surface and the potential on the body surface are used to update the boundary conditions and calculate the wave forces, respectively. As the wave-body interaction is a coupled problem, one possible way to decouple this relationship is the implementation of an iteration procedure.

In the case of a moving body, $\vec{\xi}(t+\Delta t)$, $\dot{\vec{\xi}}(t+\Delta t)$ and $\ddot{\vec{\xi}}(t+\Delta t)$ are available for the evaluation of the coefficient on both sides of the incremental motion equation for the floating body. Additionally, the increment in displacement $\delta\vec{\xi}(t+\Delta t)$ is defined to determine the termination of the iteration loop, which can be expressed for the floating body as follows:

$$\begin{aligned}&\left[\frac{4}{\Delta t^2}\boldsymbol{M}+\frac{2}{\Delta t}\boldsymbol{B}+\boldsymbol{C}\right]\delta\vec{\xi}(t+\Delta t)=\vec{F}(t+\Delta t)-\\ &\left[\boldsymbol{M}\ddot{\vec{\xi}}(t+\Delta t)+\boldsymbol{B}\dot{\vec{\xi}}(t+\Delta t)+\boldsymbol{C}\vec{\xi}(t+\Delta t)\right].\end{aligned} \quad (17)$$

Step 4: With the predicted increment in displacement, the body displacement $\vec{\xi}(t+\Delta t)$, velocity $\dot{\vec{\xi}}(t+\Delta t)$ and acceleration $\ddot{\vec{\xi}}(t+\Delta t)$ at time t+Δt are corrected as follows:

$$\left.\begin{aligned}\vec{\xi}(t+\Delta t) &= \vec{\xi}(t+\Delta t)+\delta\vec{\xi}(t+\Delta t)\\ \dot{\vec{\xi}}(t+\Delta t) &= \dot{\vec{\xi}}(t+\Delta t)+\frac{2}{\Delta t}\delta\vec{\xi}(t+\Delta t)\\ \ddot{\vec{\xi}}(t+\Delta t) &= \ddot{\vec{\xi}}(t+\Delta t)+\frac{4}{\Delta t^2}\delta\vec{\xi}(t+\Delta t)\end{aligned}\right\}. \quad (18)$$

On the free surface, the fourth-order Adams-Moulton method is used to correct the wave elevation and velocity potential as follows:

$$\left.\begin{aligned}\phi_s(t+\Delta t) &= \phi_s(t)+\frac{\Delta t}{24}\left[9f(t+\Delta t)+19f(t)-\right.\\ &\left.5f(t-\Delta t)+f(t-2\Delta t)\right]\\ \eta_s(t+\Delta t) &= \eta_s(t)+\frac{\Delta t}{24}\left[9g(t+\Delta t)+19g(t)-\right.\\ &\left.5g(t-\Delta t)+g(t-2\Delta t)\right]\end{aligned}\right\}. \quad (19)$$

We define the difference values of displacement, scattered potential and elevation at the time t+Δt as $\delta\vec{\xi}$, $\Delta\phi_s$ and $\Delta\eta_s$, then go back to Step 3 and execute the iteration until they are small enough. Go to Step 2 for a new time step.

Furthermore, the velocity potential and wave elevation of the incident wave are expressed as:

$$\phi_i=\frac{gA}{\omega}\frac{\cosh k(z+d)}{\cosh kd}\times\sin(kx\cos\beta+ky\sin\beta-\ \omega t), \quad (20)$$

$$\eta_i=A\cos(kx\cos\beta+ky\sin\beta-\ \omega t), \quad (21)$$

where η_i denotes the incident wave elevation; k denotes the wave number; ω denotes the wave frequency and A denotes the wave amplitude.

3 Model validation

For the purpose of validation, a 2-D numerical model is applied to solve the radiation problem, while a 3-D numerical model is applied for the diffraction problem. In the 2-D numerical model, the governing equation and boundary conditions are the same as those in the 3-D model with the exception that the Green's function in the 2-D model has the following form:

$$G_1(\vec{x}_2,\vec{x}_{02})=\frac{1}{2\pi}\left(\ln R_2+\ln R_{12}\right), \quad (22)$$

where $\vec{x}_{02}=(x_0,z_0)$ and $\vec{x}_2=(x,z)$ denote the source point and the field point in the 2-D model, respectively, and the expressions are as follows:

$$\left.\begin{aligned}R_2 &= \sqrt{(x-x_0)^2+(z-z_0)^2}\\ R_{12} &= \sqrt{(x-x_0)^2+(z+z_0+2d)^2}\end{aligned}\right\}. \quad (23)$$

The wave radiation around twin boxes with a gap is first investigated, and compared with the 2-D experimental results (Fredriken et al., 2014). The breadth of the box B is 36 cm, draft T is 18 cm and gap width b is 18 cm, as shown in Fig. 2. Four wave gauges are installed in the tank: two in the gap and one on each side. The wave gauges in the gap were located 6.0 cm from the hull on each side (Fig. 2 for more information). Among the two boxes, the right one is fixed and the left one undergoes a forced motion in the heave direction, specified by

$$\xi_z=A_z\cos\omega t, \quad (24)$$

where A_z denotes the forced motion amplitude and corresponding to 0.002 3 m.

The comparisons of non-dimensional wave elevations at wave gauges 1 and 2 relative to the forced motion period are shown in Fig. 3. It is observed that the present wave elevation at the wave gauge 1 agrees well with the experimental data. The frequencies of the peak wave elevations at the wave gauge 2 are coincident at T=1.175 s. However, the numerical result is overestimated when compared to the experimental data, because the energy dissipation due to the fluid viscosity is not considered in the present potential flow model.

In order to simulate the resonance amplitude more accurately, a damping coefficient μ is added to the free surface in the narrow gap. The damping coefficient is determined by the comparisons between experimental results and numerical results, which are shown in Fig. 4. According to the calculation, the coefficient μ is 0.07. Therefore, in the subsequent calculation, the results contain those with damping μ=0.07 and without damping in the free surface.

To validate the 3-D numerical model, two identical stationary rectangular barges with square bilges presented in Feng and Bai (2015) are simulated. The configuration of the side-by-side

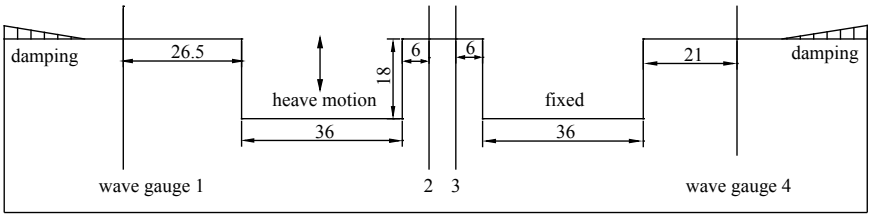

Fig. 2. Sketch of the wave radiation around two-dimensional twin boxes with a gap (unit: cm).

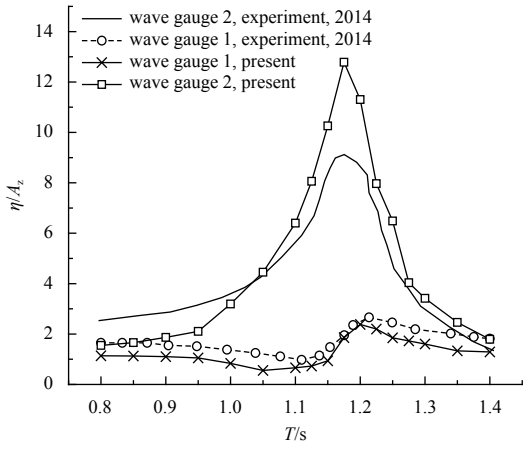

Fig. 3. Comparisons of non-dimensional wave height at wave gauges 1 and 2 for the two-dimensional wave radiation problem.

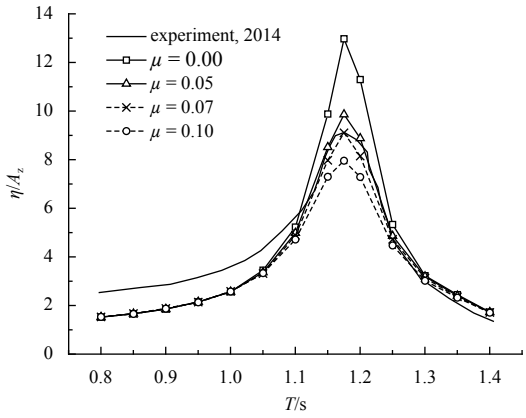

Fig. 4. Comparisons of wave height at wave gauge 2 for the two-dimensional wave radiation problem: experimental results and numerical results with different damping coefficients.

barges at the model scale is identical to that used by Feng and Bai (2015). The main parameters include a barge length L of 2.47 m, width of 0.6 m, draft D of 0.18 m and gap width 0.12 m. The water depth is set as 3 m and the beam sea situation is considered. The sway force on the up-wave barge is calculated and compared with the numerical results in Feng and Bai (2015). The symmetry of the configuration is used, and only a quadrant of the domain is considered, with 1 016 points and 350 elements on the barges, 2 512 points and 785 elements on the free water surface per quadrant, as shown in Fig. 5.

Figure 6 shows the non-dimensional sway force with a wave steepness kA=0.003 4 (same as the one in Feng and Bai (2015)). It is observed that the present results are almost identical to the

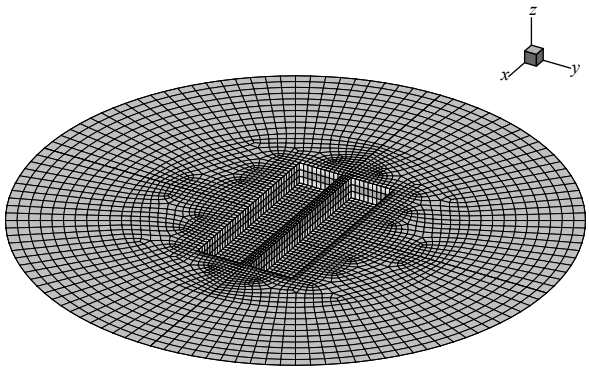

Fig. 5. 3-D meshes generated for the water interaction with two fixed side-by-side barges.

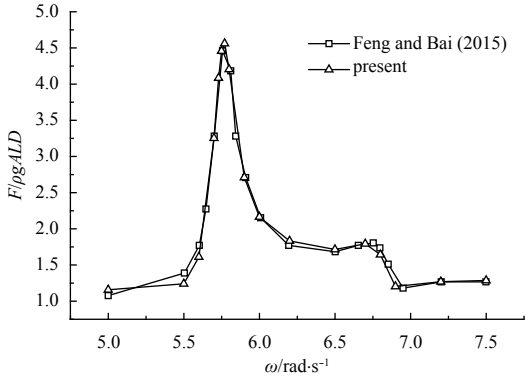

Fig. 6. Comparison of maximum sway force on the up-wave barge in the beam sea. F is the sway force on the up-wave barge.

results of the fully nonlinear numerical model over the range of simulated wave frequency.

4 Influence of up-wave barge motion on the wave elevation in the gap

When a ship berths in front of the wharf or two side-by-side ships are moored adjacently in beam seas, the up-wave barge moves in waves. In this situation, the influence of up-wave barge motion on the wave elevation in the gap may be significant, and this is investigated in the section. The two barges considered here are not identical, and the moving up-wave barge is relatively smaller than the fixed back-wave one, as shown in Fig. 7a. The specific dimensions are defined in Table 1. In addition, the up-wave barge is constrained by the linear spring with the stiffness k_{11} and k_{33} being 100 N/m

First, the floating up-wave barge is located at the middle of the fixed back-wave barge as shown in Fig. 7a. Figure 7b shows the computational mesh with 835 points and 291 elements on the

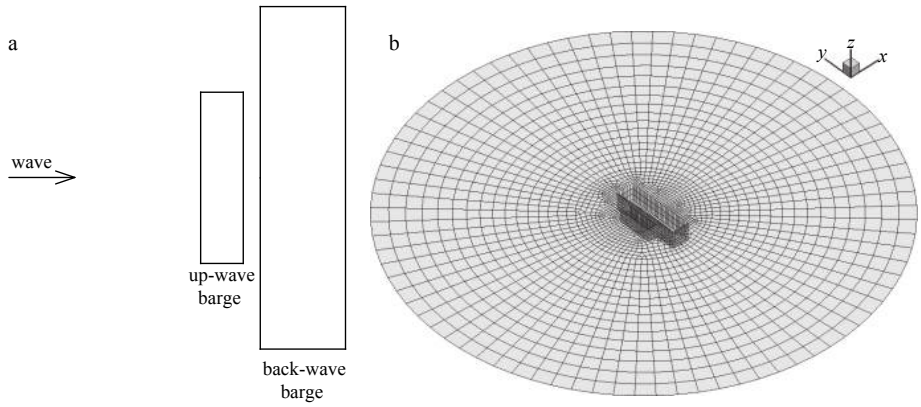

Fig. 7. Numerical simulation of the case with a moving up-wave barge in the middle. a. Sketch diagram, and b. 3-D mesh diagram.

Table 1. The parameters of the up-wave and back-wave barges

	Length/m	Width/m	Draft/m	Gravity center height/m	Rotation center height/m	Gap width/m
Up-wave barge	1.2	0.3	0.4	–0.2	–0.2	0.12
Back-wave barge	2.4	0.6	0.4	–0.2	–0.2	

barges, 3 485 points and 1 109 elements on the free water surface in the harf domain per half. The dimensionless maximum wave amplitude (with and without damping coefficient μ=0.07 in the free surface) in the gap at the midpoint is shown in Fig. 8 as the function of incident wave frequency, in which η_{cr} denotes the crest value of fluid in the gap. Compared with the case of the fixed up-wave barge, it is noted that the resonance frequency shifted to a high frequency and the maximum wave amplitude is also significantly reduced in the case of the floating up-wave barge. The decrease in the resonant wave amplitude is due to the absorption of wave energy through the movement of up-wave barge, leading to less wave energy entering the gap. Furthermore, a relatively less volume of fluid flows into the gap due to the reduction in the wave energy in the narrow gap, and this causes the movement of the resonance frequency to a high frequency. The contours of the surface elevation near the barges at resonance mode are displayed in Fig. 9 and depict comparisons of wave elevation.

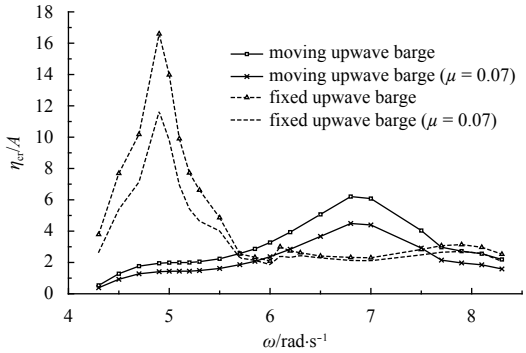

Fig. 8. Dimensionless maximum wave amplitude in the gap at the midpointin the case with the fixed and moving up-wave barges in the middle (with and without damping coefficient μ in the free surface).

In summary, the movement of the up-wave barge significantly influences the resonance wave amplitude and frequency in the gap.

Subsequently, the up-wave barge is aligned with one side of the fixed back-wave barge, as shown in Fig. 10a. In this case, the computational mesh shown in Fig. 10b includes 2 608 points and 921 elements on the barges, 5 436 points and 1 741 elements on the free water surface. The maximum wave amplitude (with and without damping coefficient μ=0.07 in the free surface) in the gap is shown in Fig. 11, which shares the similar trend as in Fig. 8, and the same reasons can explain. Furthermore, the contours of surface elevation near the barges at resonance mode are dis-

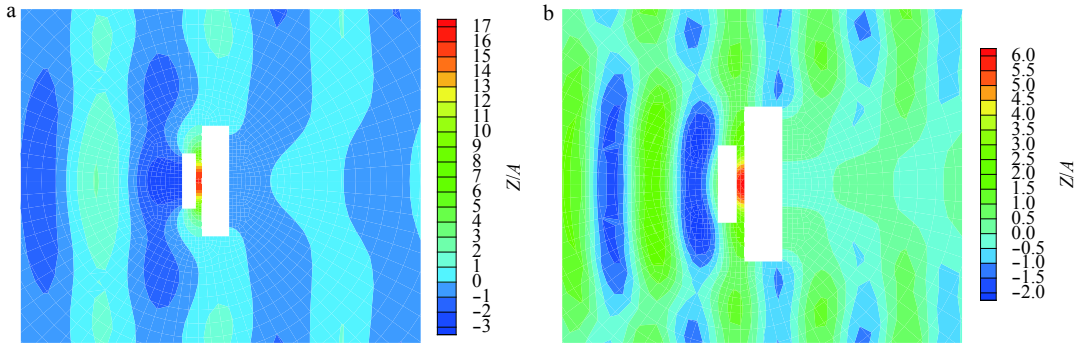

Fig. 9. Contours of surface elevation near the barges in resonance mode in the case with fixed and moving up-wave barges in the middle. a. Fixed up-wave barge, ω_a=4.90 rad/s; and b. moving up-wave barge, ω_b=6.80 rad/s.

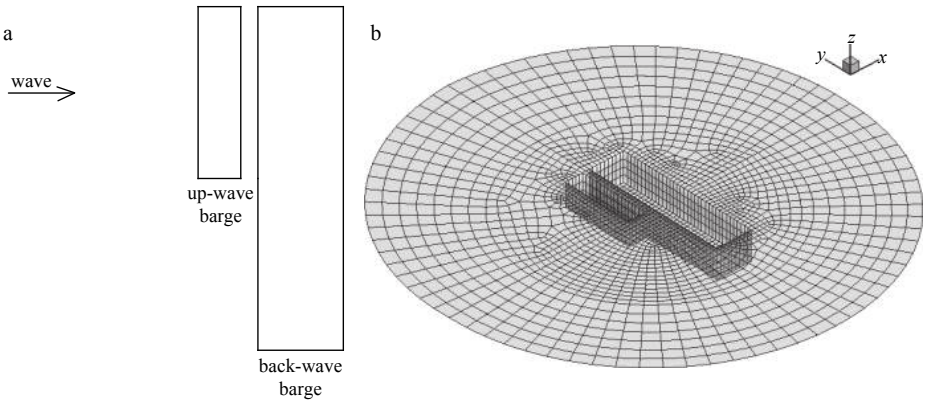

Fig. 10. Numerical simulation of the case with the moving up-wave barge aligned with one side of the back-wave barge. a. Sketch diagram, and b. 3-D mesh diagram.

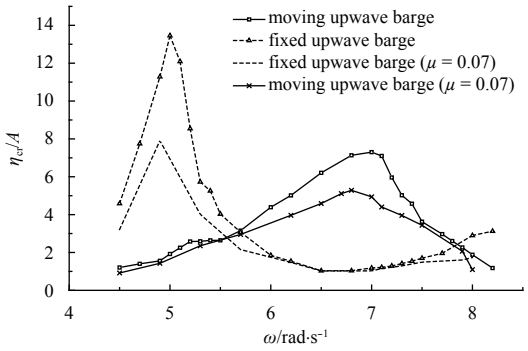

Fig. 11. Dimensionless maximum wave amplitude in the gap at the midpointin the case with fixed and moving up-wave barges aligned with one side of the back-wave barge (with and without damping coefficient μ in the free surface).

played in Fig. 12. However, the reduction in the resonance wave amplitude is less significant when compared to the case of floating up-wave barge in the middle.

The influences of the position of the up-wave barge on the maximum wave amplitude in the narrow gap and the surge motion of up-wave barge, are shown in Figs 13 and 14, respectively. It is observed that when the up-wave barge is located at the middle of the back-wave barge, both the maximum wave amplitude in the narrow gap and the surge motion of up-wave barge decrease when compared to the case of the up-wave barge aligned with one side of the back-wave barge. It suggests that the placement of the up-wave barge in the middle of back-wave barge provides more favourable hydrodynamic features for the two-body system.

The previous simulations are based on the condition of two barges with same drafts. In order to reflect the influence of drafts on the gap resonance, the draft of up-wave barge is maintained as constant (i.e., T_1=0.4 m), and three drafts of back-wave barge, i.e., T_2=0.2 m, 0.4 m and 0.8 m, are considered in the present study. The results for the distribution of surface crest at the gap are shown in Figs 15 and 16 with two positions of up-wave barge, respectively. It is observed that when the draft of the back-wave barge is smaller than the up-wave one, the resonance frequency moves to a higher frequency and the resonance amplitude will be larger. Conversely, there are less changes for resonance frequency and resonance amplitude.

5 Conclusions

In this study, the influences of the motion and location of the up-wave barge on the water resonance in the gap between two side-by-side barges are numerically investigated based on the time-domain potential flow model. A relatively small floating up-

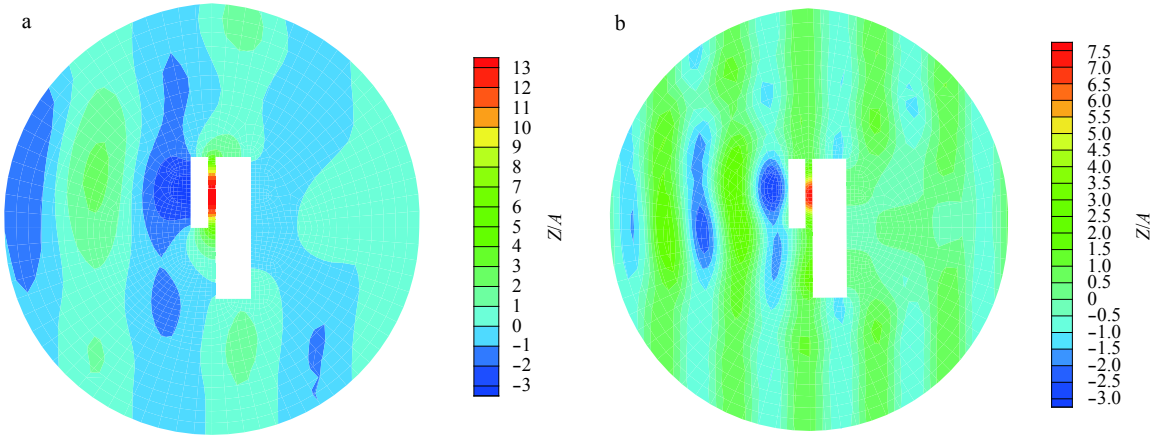

Fig. 12. Contours of surface elevation near the barges at resonance mode in the case with fixed and moving up-wave barges aligned with one side of the back-wave barge. a. Fixed up-wave barge, ω_a=5.0 rad/s; and b. moving up-wave barge, ω_b=6.80 rad/s.

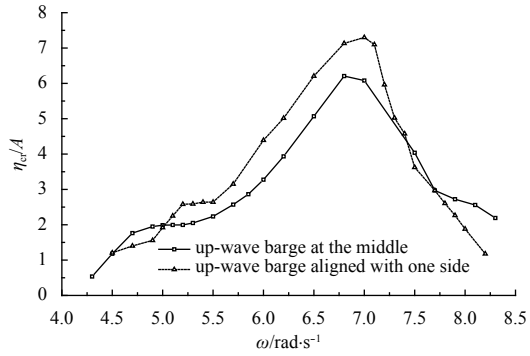

Fig. 13. Dimensionless maximum wave amplitude in the gap at the midpointin the cases with the moving up-wave barge at the middle and aligned with one side of the back-wave barge.

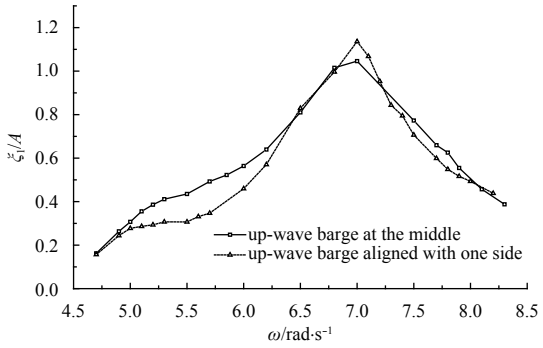

Fig. 14. Dimensionless surge motion of up-wave barge in the cases with the moving up-wave barge at the middle and aligned with one side of the back-wave barge.

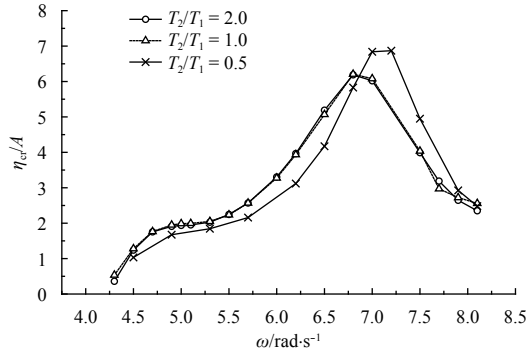

Fig. 15. Dimensionless maximum wave amplitude in the gap at the midpoint in the case with the up-wave barge and different draft back-wave barges in the middle.

wave barge and a relatively large fixed back-wave barge subjected to regular wave conditions are simulated. The results indicate that the resonance frequency increases to a higher frequency when the up-wave barge moves, and the resonance wave amplitude is significantly reduced irrespective of whether the up-wave barge is at the middle or aligned with one side of the back-wave barge. Additionally, when the up-wave barge is located in the middle of the back-wave barge, the resonance wave amplitude in the narrow gap and the motion of the up-wave barge are smaller than the case of the up-wave barge aligned with one side of the back-wave barge. Furthermore, the back-wave barge draft

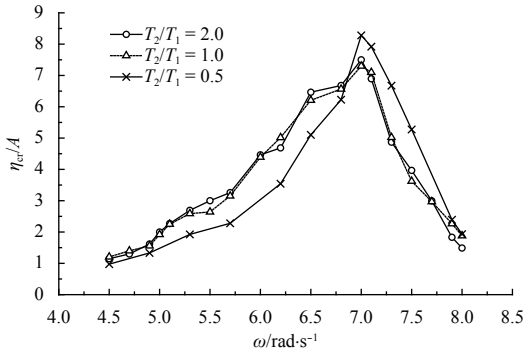

Fig. 16. Dimensionless maximum wave amplitude in the gap at the midpoint for the case with up-wave barge aligned with one side of the different draft back-wave barges.

also influence on the resonance wave amplitude and frequency in the gap. All the research results provide helpful recommendations for the narrow gap resonance phenomenon in fluid hydrodynamics research.

References

Bunnik T, Pauw W, Voogt A. 2009. Hydrodynamic analysis for side-by-side offloading. In: Proceedings of the Ninth International Offshore and Polar Engineering Conference. Osaka, Japan: ISOPE, 648–653

Chen Xiaobo. 2004. Hydrodynamics in offshore and naval applications. In: Proceeding of the 6th International Conference on Hydrodynamics (Keynote lecture). Perth, Australia: Taylor & Francis Group

Feng Xingya, Bai Wei. 2015. Wave resonances in a narrow gap between two barges using fully nonlinear numerical simulation. Applied Ocean Research, 50: 119–129

Iwata H, Saitoh T, Miao G P. 2014. Experimental and numerical investigation of wave resonance in moonpools at low forward speed. Applied Ocean Research, 47: 28–46

Iwata H, Saitoh T, Miao Guoping. 2007. Fluid resonance in narrow gaps of very large floating structure composed of rectangular modules. In: Proceedings of the Fourth International Conference on Asian and Pacific Coasts. Nanjing: International Society of Asian and Pacific Coasts, 815–826

Jiang Shengchao, Tang Peng, Zou Li, et al. 2017. Numerical simulation of fluid resonance in a moonpool by twin Rectangular hulls with various configurations and heaving amplitudes. Journal of Ocean University of China, 16(3): 422–436

Jin Ruijia, Teng Bin, Ning Dezhi, et al. 2017. Numerical investigation of influence of wave directionality on the water resonance at a narrow gap between two rectangular barges. Acta Oceanologica Sinca, 36(6): 104–111

Kristiansen T, Faltinsen O M. 2012. Gap resonance analyzed by a new domain-decomposition method combining potential and viscous flow DRAFT. Applied Ocean Research, 34: 198–208

Li Shu, Teng Bin. 2015. Numerical examination of wave-induced coupling roll motion and fluid resonance between twin floating barges in proximity. Procedia Engineering, 126: 242–246

Liu Yong, Li Huajun. 2014. A new semi-analytical solution for gap resonance between twin rectangular boxes. Journal of Engineering for the Maritime Environment, 228(1): 3–16

Lu Lin, Chen Xiaobo. 2012. Dissipation in the gap resonance between two bodies. In: Eatock T R, Grue J, Molin B, eds. The 27th International Workshop on Water Waves and Floating Bodies. Copenhagen: Denmark, 22–25

Lu Lin, Cheng Liang, Teng Bin, et al. 2010. Numerical investigation of fluid resonance in two narrow gaps of three identical rectangular structures. Applied Ocean Research, 32(2): 177–190

Lu Lin, Teng Bin, Sun Liang, et al. 2011. Modelling of multi-bodies in

close proximity under water waves-Fluid forces on floating bodies. Ocean Engineering, 38(13): 1403–1416

Miao Guoping, Ishida H, Saitoh T. 2000. Influence of gaps between multiple floating bodies on wave forces. China Ocean Engineering, 14(4): 407–422

Miao Guoping, Ishida H, Saitoh T. 2001. Water wave interaction of twin large scale caissons with a small gap between. Coastal Engineering Journal, 43(1): 39–58

Molin B, Remy F, Camhi A, et al. 2010. Experimental and numerical study of the gapresonances in-between two rectangular barges. Journal of Experimental Marine Biology & Ecology, 30(50): 2521–2523

Moradi N, Zhou Tongming, Cheng Liang. 2015. Effect of inlet configuration on wave resonance in the narrow gap of two fixed bodies in close proximity. Ocean Engineering, 103: 88–102

Newman J N, Sclavounos P D. 1988. The computation of wave loads on large offshore structures. In: Proceeding of International Conference on Behavior of Offshore Structure (Boss). Trondheim: International Society of Behavior of Offshore Structure, 605–622

Newman J N. 2004. Progress in wave load computations on offshore structures. In: Proceedings of the 23rd Conference on Offshore Mechanics and Arcitc Engineering. California: American Society of Mechanical Engineers, 20–25

Pauw W H, Huijsmans R, Voogt A. 2007. Advances in the hydrodynamics of side-by-side moored vessels. In: Proceedings of the 26th Conference on Offshore Mechanics and Arcitc Engineering. San Diego, California, USA: American Society of Mechanical Engineers, 597-603

Perić M, Swan C. 2015. An experimental study of the wave excitation in the gap between twoclosely spaced bodies, with implications for LNG offloading. Applied Ocean Research, 51: 320–330

Sun Liang, Taylor R E, Taylor P H. 2010. First- and second-order analysis of resonant waves between adjacent barges. Journal of Fluids and Structures, 26(6): 954–978

Watai R A, Dinoi P, Ruggeri F, et al. 2015. Rankine time-domain methodwith application to side-by-side gap flow modeling. Applied Ocean Research, 50: 69–90

Yeung R W, Seah R K M. 2006. On the Behavior of Twin-Body Heave Hydrodynamic Coefficients. In: The 26th International Offshore and Polar Engineering Conference. San Francisco, California: International Society of Offshore and Polar Engineers, 291–296